The Delayed Response of Airborne Thermometers: Part 1: Determining the Transfer Function

William A. Cooper and others...

DRAFT April 2020

National Center for Atmospheric Research
Earth Observing Laboratory
Research Aviation Facility

Table of Contents

List of Figures

List of Tables

Preface and Abstract

This is Part 1 of a three-part series addressing errors that are present in most archived measurements of temperature made from research aircraft. In this first part, the time response of standard airborne thermometers is quantified by determining the transfer function where the known input is turbulent dynamic heating. Differential equations for the response are proposed, and it is verified that the solutions to those differential equations provide good representations of the response characteristics in terms of fitted empirical coefficients. Those solutions then can be used to correct the measurements to compensate in part for the response characteristics of the sensors. Part 2 will use these results to demonstrate that standard data processing used by most operators of research aircraft introduces errors that arise from incorrect adjustment for dynamic heating. Part 3 will use the results from the first two papers to assess how these errors affect measurements of the flux of sensible heat and will propose and evaluate a method for correcting those measurements that removes a significant error in that measured flux.

Acknowledgements

This material is based upon work supported by the National Center for Atmospheric Research, which is a major facility sponsored by the National Science Foundation under Cooperative Agreement No. 1852977. Any opinions, findings and conclusions or recom-mendations expressed in this publication are those of the author(s) and do not necessarily reflect the views of the National Science Foundation. Measurements used here (UCAR/NCAR - Earth Observing Laboratory [2011], UCAR/NCAR - Earth Observing Laboratory [2019], UCAR/NCAR - Earth Observing Laboratory [2018]) were collected in research projects (Wood et al. [2011], Albrecht et al. [2019], McFarquhar et al. [2014]) that used the NSF/NCAR research aircraft. Project descriptions and additional information can be found at this URL. The referenced project teams conducted the experiments, with flight operations, data acquisition and processing, and other project support by the Research Aviation Facility, Earth Observing Laboratory, National Center for Atmospheric Research (NCAR). The analyses reported here were mostly performed using R (R Core Team [2019]), with RStudio (RStudio [2009]) and knitr (Xie [2013, 2014]). Data files in netCDF format have been read and written using the R package "ncdf4"; cf. Pierce [2015]. Substantial use also was made of the "ggplot2" package (Wickham [2009]) for R, and extensive use was made of the "stats" package, part of Core R. Some of the numerical integrations used the Runge-Kutta function from the "rmutil" package (Swihart and Lindsey [2019]).

1 Introduction

Research aircraft routinely measure the air temperature, but the standard sensors do not respond fast enough to meet many scientific needs. In particular, measurements of the flux of sensible heat need faster response than is typically available, as do measurements of near-discontinuous changes such as those at the top of boundary layers or at cloud boundaries. The measurement of sensible-heat flux requires, for the standard eddy-correlation measurement, that temperature be measured with sufficient response to resolve the spectrum of contributions to the flux. Various recent reviews of priorities for research in atmospheric science have called attention to the important roles that fluxes of various quantities play in climate science and have advocated increased focus on those fluxes; e.g., National Research Council [1998].

The basis for the measurement of the flux of sensible heat (F_s) by eddy correlation is this equation:

$$F_s = \rho_a C_p \left\langle w'T' \right\rangle \tag{1}$$

where ρ_a is the density of air, C_p the specific heat of air at constant pressure, w the vertical wind, and T the temperature. Primes in this equation denote fluctuations from the mean and angle brackets denote an ensemble average. The measurement thus depends on having a temperature sensor that can respond to the range of fluctuations making significant contributions to the heat flux. Friehe and Khelif [1992] suggested that 4–5 Hz is "just adequate" (for flight at around 125 m/s) and that 25 Hz would be desirable to resolve some interesting aspects of the temperature structure. If the response of the temperature sensor is reduced or shifted in phase at a particular frequency, an error will be introduced into the measurement of sensible-heat flux. Lawson and Rodi [1992] argued that sensible-heat flux measured by some of the fastest sensors then in common use produced measurements of sensible heat flux about 21% too low compared to the measurements from their faster thermocouple-based sensor. To avoid significant errors in this measurement, it therefore is essential to characterize the time response of the temperature sensor used and, where necessary, to apply corrections to compensate for that response.

In this first paper, the time response of some standard airborne temperature sensors is characterized in terms of a transfer function that relates the measurand (the recovery temperature) to the measurement (the sensor output) in ways that are invertible. Two coupled differential equations are used as the basis for this characterization, but the transfer function is determined independent of those equations. Because the equations predict a transfer function matching the observations, they provide a useful generalization when the measurements are fitted to a three-parameter equation consistent with those equations. The measured transfer functions for standard airborne thermometers then are used in the papers that follow to access how common measurements are affected.

2 Theory

The errors considered here apply to the measurement from the sensor, the "recovery temperature," rather than the final temperature after correction for dynamic heating. Because the sensor cannot respond to rapid fluctuations, the standard correction for dynamic heating introduces errors into the measured air temperature that are then amplified by a correction procedure. This will be addressed in Part 2, but for this reason the present paper will discuss only the recovery temperature.

Payne et al. [1994] provided a particularly illuminating analysis of the expected response of a temperature sensor and developed their results in terms of a transfer function. They represent the response of the sensor in terms of two coupled differential equations, one representing the temperature of the sensing wire and a second representing the temperature of the structure that supports that wire. Their analysis in terms of fundamental representation of the heat transport leads to reasonable consistency with previous two-time-constant models like that of McCarthy [1973] but poor agreement with the empirical evidence regarding the time-response parameters in those models. They note, however, that the empirical evidence is not as consistent or convincing as would be desirable. One goal of the present work is to develop a different and readily available method of determining those parameters. The over-arching goal is to be able to assess errors that might be present in measurements of the flux of sensible heat and to apply corrections for those errors. This will be the subject of Part 3.

2.1 The differential equations and their solution

Previous studies have demonstrated that a simple first-order exponential equation with one time constant does not represent the time response of airborne temperature sensors. The suggested explanation (Lenschow [1972] is that heat is transferred to the sensing wire of standard sensors not only from the air but also from the supporting structure that is in contact with the wire. Friehe and Khelif (Friehe and Khelif [1992]), following other prior work including that of Rodi and Spyers-Duran [1972] and McCarthy [1973], suggested representing the two-time-constant response via the following functional form:

$$\Theta(t) = A_1 e^{-t/\tau_1} + A_2 e^{-t/\tau_2} \tag{2}$$

where $\Theta(t)$ is the normalized history of the measured temperature decaying from an initial value of unity to a final value of zero. The sum of the coefficients A_1 and A_2 must then be 1. The values for $\{A_1, A_2, \tau_1, \tau_2\}$ suggested by Friehe and Khelif [1992] were $\{0.65, 0.35, 0.09\ \text{s}, 0.5\ \text{s}\}$.

Following the approach of Payne et al. [1994], the time response of the sensor will be represented by two coupled differential equations, one that describes the response of the support on which the sensing wire is wound to the air temperature and a second that describes the response of the sensing wire to two inputs, one from the support and one from the air. No attempt is made here to determine the parameters from first principles as in Payne et al. [1994], however; instead, parameters entering the equations are determined empirically. The equations are:

$$\frac{dT_s(t)}{dt} = \frac{T_r(t) - T_s(t)}{\tau_2} \tag{3}$$

$$\begin{aligned}\frac{dT_m(t)}{dt} &= \frac{a(T_r(t) - T_m(t)) + (1-a)(T_s(t) - T_m(t))}{\tau_1} \\ &= \frac{\{aT_r(t) + (1-a)T_s(t)\} - T_m(t)}{\tau_1}\end{aligned} \tag{4}$$

where $T_s(t)$ is the temperature of the support, $T_m(t)$ the measured temperature of the sensing wire, and $T_r(t)$ the true recovery temperature that is the measurand. For heat transfer to or from the wire, the parameter a then represents the fraction of the heat transferred by the air, while $(1-a)$ is transferred to or from the support. The wire responds to the combined transfers of heat with characteristic time constant τ_1 while the support structure responds to the air temperature more slowly, with time constant τ_2. It is straightforward to apply (3) and (4) to changing but not necessarily discrete conditions, so a general response to a given air-temperature history can be predicted by numerical integration of these equations. Furthermore, the equations are linear and, for constant values of the parameters, they are also time-invariant (i.e., "LTI") descriptions of the response. As a result, a particular signal for $T_r(t)$ can be decomposed into its sinusoidal Fourier components and each will satisfy these equations independently. The first equation does not involve the measurement, so for a particular history of recovery temperature $T_r(t)$ the support temperature can be determined solely by integration of (3). Then, with $T_s(t)$ determined, (4) can be integrated to find the expected measurement $T_m(t)$ for a specified measurand history $T_r(t)$. The inverse process, finding $T_r(t)$ from the measurements $T_m(t)$, is also straightforward and only slightly more complicated, as discussed in Appendix A.

For a sinusoidal input these equations have analytic solutions after any transient response from initial conditions has decayed. If the actual recovery temperature is $T_r(t) = \sin \omega t$ where ω is the angular frequency, then the solutions for $T_s(t)$ and $T_m(t)$ are given by the following equations:

$$T_s(t) = b \sin(\omega t + \zeta) \tag{5}$$

$$T_m(t) = c \sin(\omega t + \phi) = C_1 \cos \omega t + C_2 \sin \omega t \tag{6}$$

where

$$b = \frac{1}{\sqrt{1 + \omega^2 \tau_2^2}}$$

$$\zeta = -\arctan(\omega \tau_2)$$

$$\begin{aligned}C_1 &= \left(\frac{1}{1 + \omega^2 \tau_1^2}\right)(-\omega \tau_1 (a + (1-a) b \cos \zeta) + (1-a) b \sin \zeta) \\ &= \frac{-\omega}{(1 + \omega^2 \tau_1^2)}\left(\tau_1 a + \frac{(1-a)(\tau_1 + \tau_2)}{(1 + \omega^2 \tau_2^2)}\right)\end{aligned}$$

$$C_2 = \left(\frac{1}{1+\omega^2\tau_1^2}\right)(a+(1-a)b\cos\zeta+\omega\tau_1(1-a)b\sin\zeta)$$
$$= \left(\frac{1}{1+\omega^2\tau_1^2}\right)\left(a+\frac{(1-a)(1-\omega^2\tau_1\tau_2)}{(1+\omega^2\tau_2^2)}\right)$$

$$c = \sqrt{C_1^2+C_2^2} \tag{7}$$

$$\phi = \arctan(C_1/C_2) \tag{8}$$

McCarthy [1973] used the derivative of the step-function response to find the impulse response function and, from its Fourier transform, the sensor response function. That leads to the following alternate expressions for C_1 and C_2:

$$C_1 = -\omega\left(\frac{A_1\tau_1}{1+\omega^2\tau_1^2}+\frac{A_2\tau_2}{1+\omega^2\tau_2^2}\right)$$
$$C_2 = \left(\frac{A_1}{1+\omega^2\tau_1^2}+\frac{A_2}{1+\omega^2\tau_2^2}\right)$$

With $A_2 = (1-a)/(1-\tau_1/\tau_2)$ and $A_1 = 1-A_2$, these are equivalent to the expressions for the same coefficients given above (7). This demonstrates that the equations (3) and (4) are a representation of the response equivalent to (2) and to the equations used by McCarthy [1973] and Inverarity [2000], among others.

2.2 The transfer function

The transfer function $H(\omega) = c(\omega)e^{i\phi(\omega)}$ then characterizes how the sensor will respond to a unit-amplitude sine wave with angular frequency $\omega = 2\pi\nu$ where ν is the frequency. For a particular set of parameters (a =0.733, τ_1 =0.0308 s, τ_2 =0.447 s),[1] the amplitude response and phase delay of the transfer function is shown in Fig. 1. Similar plots of the amplitude (but not the phase) have been shown by McCarthy [1973] and Nicholls [1978]. Modified transfer functions for two small changes to these parameters are also shown to illustrate the sensitivity of the solution to these parameters. This figure illustrates that serious errors will enter estimates of the sensible heat flux if temperature fluctuations at frequencies above 1 Hz make a significant contribution to the flux. The contribution to the cospectrum of temperature and vertical wind will be reduced by the product of the amplitude and the cosine of the phase (Fig. 2). Most of the 10-Hz contribution is missed, but even at 1 Hz the error is about 28%.

These equations and their solution provide a basis for correcting either the measured temperature or the sensible-heat flux calculated from the cospectrum in (1). Corrected values can be obtained by several methods including integration of the equations for the derivatives or by dividing the Fourier transform of the time series by the transfer function and then using inverse Fourier transformation to recover the corrected time series. Those correction schemes are discussed in detail in Appendix A. To support such corrections, the next section determines the transfer function experimentally.

[1] These parameters are approximately representative of an unheated Rosemount 102E4AL sensor used on the NSF/NCAR C-130, as will be demonstrated in Sect. (3.2.1).

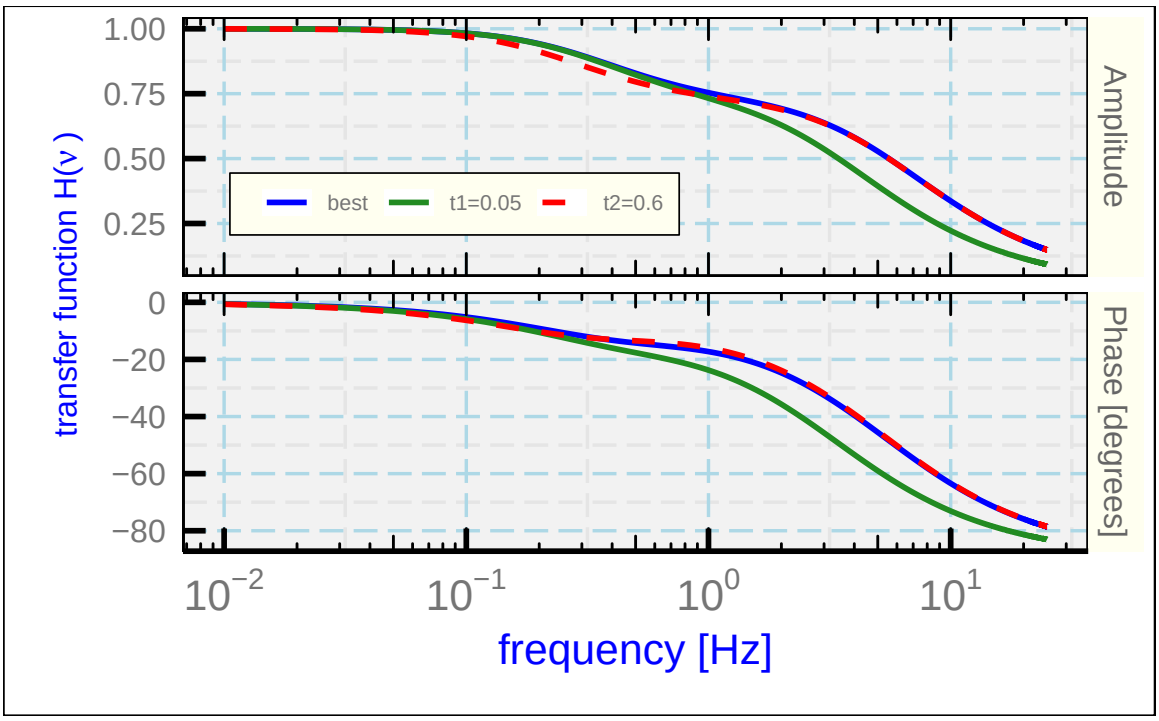

Figure 1: The amplitude and phase for the frequency domain transfer function of the Rosemount 102E4AL temperature sensor. The parameters representing that sensor, labeled "best", are a=0.733, $\tau_1 = 0.0308$ s and $\tau_2 = 0.447$ s. To illustrate sensitivity, the curves labeled "t1=0.05" and "t2=0.6" use instead $\tau_1 = 0.05$ s and $\tau_2 = 0.6$ s, respectively.

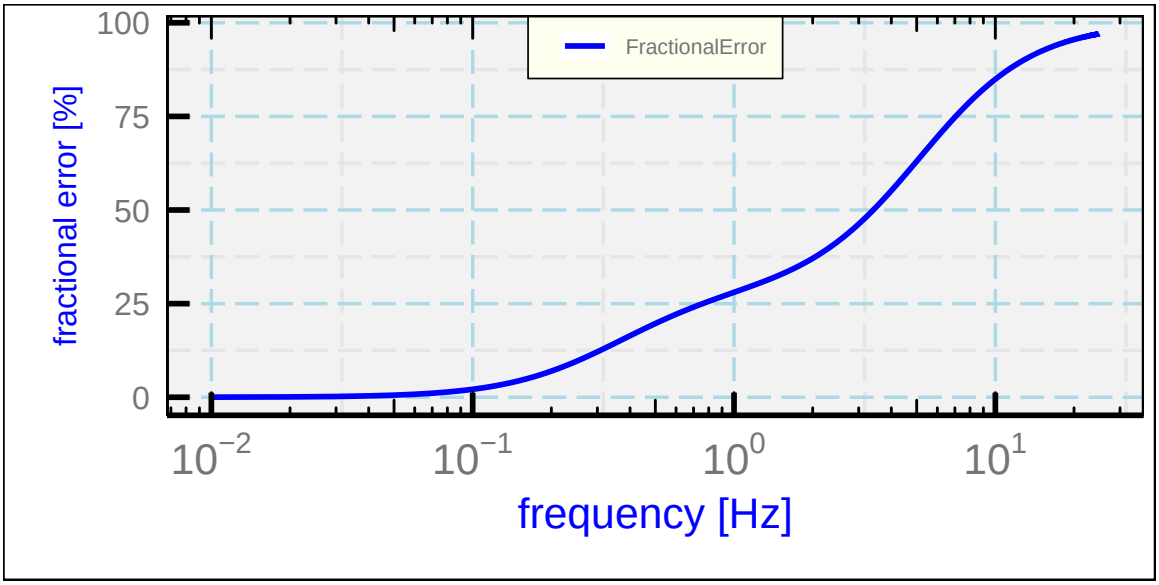

Figure 2: Fractional error in the cospectrum of sensible-heat flux caused by the delayed response of the Rosemount 102E4AL temperature sensor.

3 Determining the Tranfer Function

The evaluation of the time response that follows relies on the dynamic heating produced by airspeed fluctuations. In steady conditions a temperature sensor exposed to the air stream will measure the recovery temperature, defined as the ambient temperature increased by the effect of dynamic heating. Dynamic heating fluctuates as the airspeed fluctuates, so in a turbulent wind field fluctuations with a measurable frequency spectrum are imposed on the sensor. These fluctuations are often significantly larger than real fluctuations in the ambient temperature. Dynamic heating of temperature sensors is discussed for example by Bange et al. [2013] (cf. their Eq. 2.23), who expresses dynamic heating Q as

$$Q = \alpha_r \frac{V^2}{2C_p} = T_r \left(\frac{\alpha_r M^2 R_a/(2C_v)}{1 + \alpha_r M^2 R_a/(2C_v)} \right) \tag{9}$$

where α_r is the "recovery factor" characterizing the extent to which the air is brought to rest relative to the sensor, V is the airspeed, C_p and C_v are respectively the specific heat of air at constant pressure and constant volume. T_r is the (true) recovery temperature expressed in absolute units, M the Mach number, and R_a the gas constant for air. The ambient air temperature T_a is related to the recovery temperature and the dynamic heating via

$$T_r = T_a + Q \ . \tag{10}$$

Because dynamic heating can exceed 20°C at jet-aircraft flight speeds, it is often the dominant cause of fluctuations in the recovery temperature. If the fluctuations in dynamic heating are higher in frequency than those to which the sensor can respond, corresponding fluctuations will be attenuated in the measured spectrum and the phase of the measured response relative to the imposed signal will vary, from near 0° for fluctuations slow compared to sensor response to near 90° or even more[2] for fluctuations fast compared to that response. The amplitude and phase of the recovery temperature relative to the dynamic-heating forcing therefore can be used as sensitive indicators of the response characteristics of the sensor and can constrain parameters like a, τ_1 and τ_2 that fit the predictions to the observations. The evaluation in terms of the amplitude ratio and phase shift of the recovery temperature in response to dynamic heating will be used to characterize the transfer function and to determine if it is represented adequately by the parameterized form given by (7) and (8).

3.1 Measurements

The present investigation uses measurements from two NSF/NCAR (National Science Foundation / National Center for Atmospheric Research) research aircraft, a Gulfstream V (hereafter, GV) and a Hercules C-130. The temperature sensors producing the measurements are in widespread use so these results should have broad applicability. Some aspects of the uncertainty limits associated with these measurements of temperature are included in an NCAR Technical Note (Cooper et al. [2016]), which focused on the measurements of wind from the

[2] A sensor with a first-order time constant cannot produce a phase lag of more than 90°, but larger lags are possible for systems characterized by two time constants, as developed below.

GV. That document included an estimate that the standard uncertainty in measurements of temperature from the GV is about 0.3°C and referenced Cooper et al. [2014] for supporting evidence. This limit applies when the temperature being measured is varying slowly but does not apply when the temperature changes rapidly. It is well known, however, that temperature sensors in common use on research aircraft have time-response characteristics that can affect the measurements. Friehe and Khelif [1992] and Lawson and Rodi [1992], among many others, provide reviews of the evidence for delayed response of the standard sensors. In particular, the unheated Rosemount 102E4AL sensor has been used widely as a fast-responding sensor, so it will be a focus of this three-part study.

This research uses data archives produced by three research projects, the VOCALS (VAMOS Ocean-Cloud-Atmosphere-Land Study), CSET (Cloud Systems Evolution in the Trades) and SOCRATES (Southern Ocean Clouds, Radiation, Aerosol Transport Experimental Study) experiments. The field projects are described by Wood et al. [2011], Albrecht et al. [2019] and McFarquhar et al. [2014], respectively. All included low-level flight segments over the Pacific Ocean that are used in this paper. The reference list includes appropriate DOI references to the measurements.

3.2 The response to dynamic heating

Because the airspeed V is itself conventionally determined using the processed air temperature T_a, via $V = M\sqrt{\gamma R_a T_a}$ where $\gamma = C_p/C_v$, the second expression in (9) provides the advantage that it does not rely on prior calculation of the air temperature T_a but can be calculated from only the recovery temperature T_r and the Mach number. The Mach number in turn depends only on measurements of the dynamic and ambient pressures, with a small adjustment for the water vapor pressure. However, the available measurement is not the true recovery temperature T_r but instead the measured temperature T_m which may not include high-frequency fluctuations in T_r. This in turn affects the estimated fluctuations determined from (9). To minimize this problem, regions were sought where the fluctuations in dynamic heating were the dominant cause of fluctuations in recovery temperature. Temporarily consider these approximations: $\alpha_r \approx 1$, $R_a/(2C_v) \approx 1/5$, and M small enough that the denominator of the right side of (9) can be assumed equal to unity. Dynamic heating then is approximately $Q \approx T_r M^2/5$ and fluctuations in Q are related to those in T_r and M according to

$$\frac{\delta Q}{Q} \approx \frac{\delta T_r}{T_r} + \frac{2}{5}\frac{\delta M}{M} \tag{11}$$

Because the measured recovery temperature T_m may not include true high-frequency fluctuations in T_r, the measured phase and amplitude of the response to the dynamic-heating term may be distorted from the correct value at frequencies where $\delta T_m/T_m$ differs from $\delta T_r/T_r$. In regions where the last term in (11) dominates, underestimation of the fluctuations in the recovery temperature arising from sensor response will cause less significant errors in the measured fluctuations in dynamic heating Q, and those errors can be addressed by correction procedures.

Figure 3 shows the contributions to the dynamic-heating term from the two terms on the right side of (11), except that T_m is used instead of the unknown T_r. This is based on a low-level

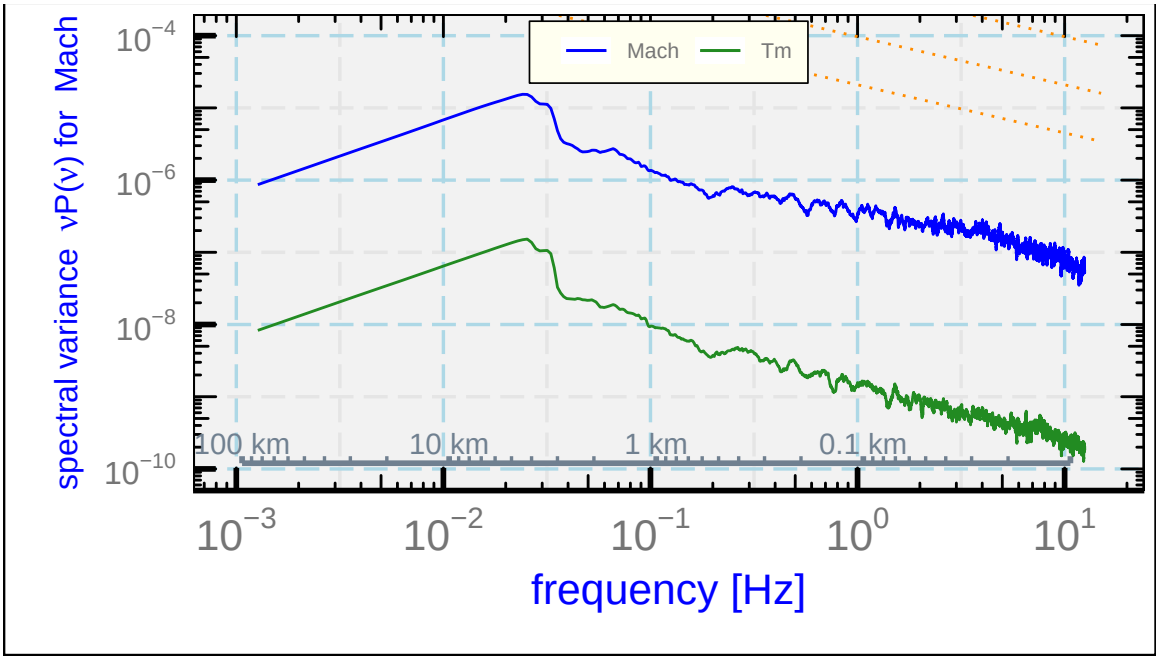

Figure 3: Frequency-weighted spectral variance for $\delta T_m/T_m$ and $0.4\delta M/M$ as functions of frequency (ν) for a low-level flight segment from VOCALS flight 3, 21 Oct 2008 11:39:00 – 11:52:00 UTC. The wavelength scale shows the correspondence between frequency and wavelength at the average airspeed. The two terms are labeled "Tm" and "Mach" in the legend.

flight segment with moderate turbulence where the airspeed fluctuations were approximately consistent with an eddy dissipation rate of $3 \times 10^{-4}\,\mathrm{m^2 s^{-3}}$. The variance of the second term is more than 100 times that of the first, indicating that the fluctuations in the first term are less than 10% of those in the second term. Therefore the right side of (9) with T_m in place of T_r was used initially to represent dynamic heating. Once a set of parameters was determined, $T_r(t)$ was calculated using the first correction procedure discussed in Appendix A. Iteration using this estimate of $T_r(t)$ in place of $T_m(t)$ led to a small change in the fitted values of the parameters, and the estimate became stable after only one iteration.

3.2.1 The unheated Rosemount 102E4AL sensor

Segment	start	end
1	6:50:00	7:00:00
2	7:33:00	7:43:00
3	10:46:00	10:56:00
4	11:42:00	11:52:00
5	12:43:00	12:53:00
6	13:30:00	13:40:00

Table 1: Flight segments from flight 3 of the VOCALS project, 21 October 2008. Listed times are UTC.

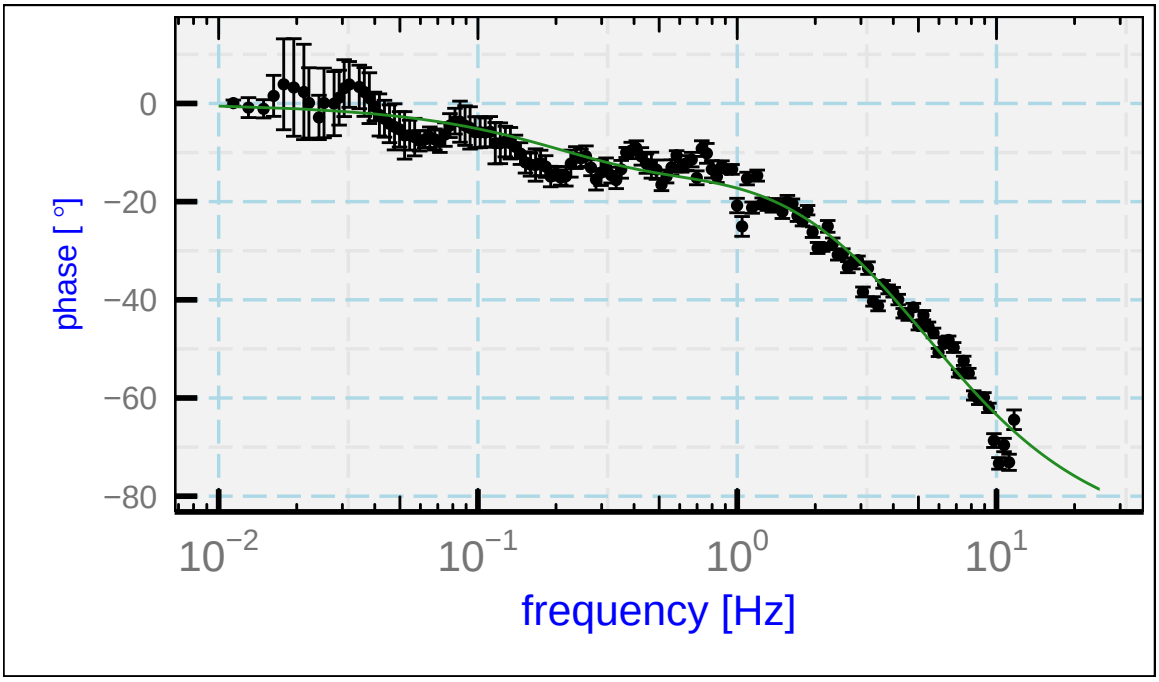

Figure 4: Phase lag of measured recovery temperature behind dynamic heating, for the measurements (with error bars) and for the theoretical response for the best-fit parameters (green line). The error bars indicate two-standard-deviation ranges in the mean at each plotted point. Data from the flight segments listed in Table 1.

To characterize the response of the Rosemount 102E4AL sensor, six ten-minute low level flight segments in the marine boundary layer from one flight of the NCAR/NSF C-130 in the "VOCALS" project (Wood et al. [2011]), which studied low-level clouds over the Pacific Ocean near Chile, were selected that had simular flight conditions including the intensity of the turbulence. The time intervals are listed in Table 1. For each flight segment, the phase and amplitude ratio between the measurement and the dynamic heating term were calculated,[3] and the results for all six segments were averaged in 200 logarithmically spaced intervals in frequency. The results for the average phase are shown in Fig. 4. The theoretical curve is based on best-fit parameters as determined from these measurements and those of the amplitude ratio, discussed next.

The ratio of the amplitude of the response to that of the dynamic-heating signal, used as an estimate of the gain of the transfer function, is shown in Fig. 5. It is useful to consider both the amplitude and phase when determining the response parameters because, as shown in Fig. 1, the amplitude of the transfer function is more sensitive to τ_2 than the phase but τ_1 is a very sensitive predictor of the phase at high frequency. For the set of favored parameters, Fig. 5 shows the standard prediction and another with τ_2 set to 0.6 s instead, to show the sensitivity of this result to that parameter. The best prediction based on the measured phases consistently underestimates the ratio of spectra for frequencies below about 0.1 Hz and above about 3 Hz but is reasonably consistent with the observed ratio between 0.1 Hz and 3 Hz. Below 0.1 Hz it appears likely that the sensor is responding to real fluctuations in temperature not attributable

[3] The R routine "spec.pgram()" was used with 25-point modified Daniell smoothing.

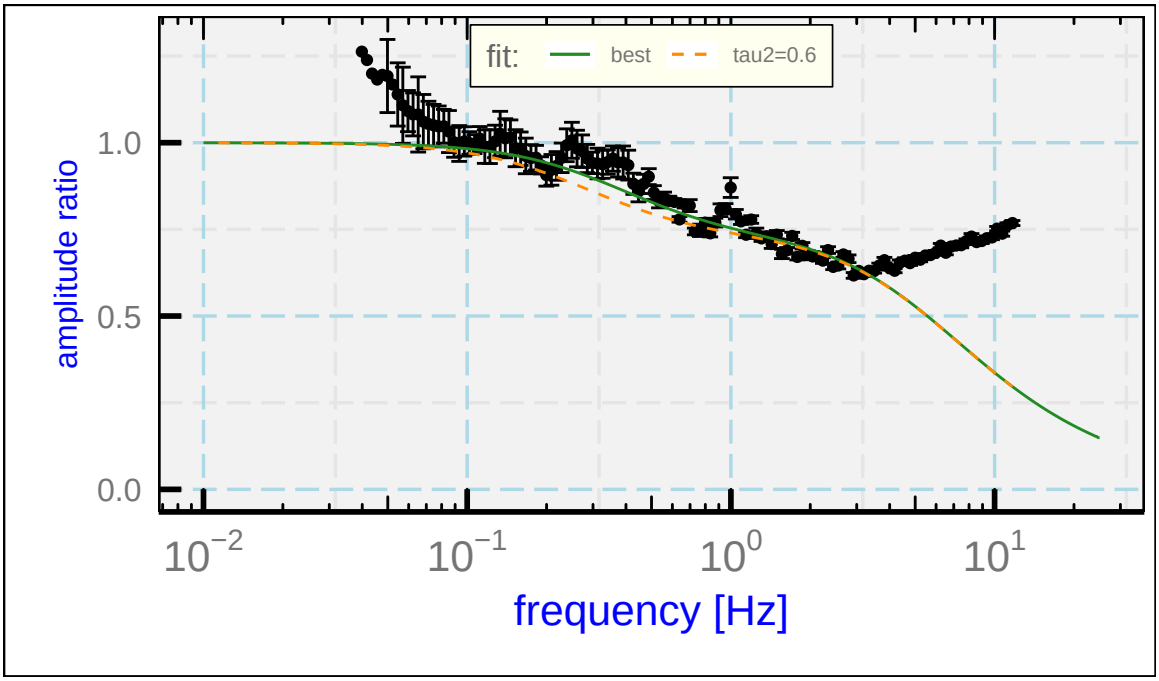

Figure 5: The ratio of the spectral amplitude for the measurement of recovery temperature ($T_m(t)$) to that for dynamic heating (Q), shown as the plotted data points. There are additional data points at frequencies below about 0.04 Hz that do not appear in this plot because they lie above the upper limit for the ordinate. The green line is the prediction from the transfer function determined from the best-fit values matching the phase lag between these variables, and the dashed orange line is a similar result with the second time constant τ_2 increased from 0.447 to 0.6 s to illustrate sensitivity to this parameter.

to dynamic heating, as would be expected at these low frequencies. Above 3 Hz the prediction is much too low, probably because there is noise or other spurious variance in $T_m(t)$ not caused by dynamic heating.

The fit procedure used (7) and (8) to find the theoretical value of the amplitude ratio and phase at each frequency represented in the observations. For assumed values of the three parameters a, τ_1 and τ_2, a chi-square was calculated from the differences between these theoretical values and the observed values. The frequencies used for the fit were 0.01 to 12 Hz for the measurements of phase and 0.1 to 3 Hz for the measurements of amplitude ratio, to avoid regions where effects other than dynamic heating appear to bias the measurements. Then a search procedure varied these parameters to seek the minimum value of the chi-square.[4] The resulting values were $a = 0.73$, $\tau_1 = 0.031$ and $\tau_2 = 0.45$. The chi-square for the fit is about 18 times larger than expected if the fit represents the measurements to measurement uncertainty, so it is difficult to assign uncertainty limits to this result on the basis of this fit because of this not-understood excess chi-square, but the fit minimum distinguished nearby values to about three significant digits in all three parameters. The Hessian from the fit implies that the results with standard uncertainties

[4]The code can be found in the "Rnw" document that generates the present document. It used the "optim()" function from the R "stats" package produced by the R Core Team [2019].

are $a = 0.733 \pm 0.004$, $\tau_1 = 0.0308 \pm 3 \times 10^{-4}$ and $\tau_2 = 0.45 \pm 0.02$.

To complete the iteration discussed earlier, the measured recovery temperature was then corrected via method 1 from Appendix A, using the parameters from this first fit, to find a prediction for the actual recovery temperature $T_r(t)$. After recalculating Q using (9) with that estimate of $T_r(t)$ in place of $T_m(t)$, the calculation of phase and amplitude was repeated and the results were fitted again by adjusting the fit parameters. Only very minor changes arose from this procedure even after one iteration, but the iterated result is the one used here to represent the unheated Rosemount 102E4AL sensor.

The airflow and typical flow angles approaching a sensor can affect its response, so the results might change when installed on a different location or a different aircraft. Therefore a similar evaluation examined the response of this same sensor when flown on the NSF/NCAR GV, which flies significantly faster than the C-130. The results of a study using a combined low-level dataset from the SOCRATES (McFarquhar et al. [2014]) and CSET (Albrecht et al. [2019]) experiments, which were flown over the Pacific Ocean, were similar to but slightly different from the coefficients determined on the C-130, with both time constants a little smaller than found for the C-130 (τ_1 =0.024 and τ_2 =0.22). This might be expected at greater airspeed, as discussed in Sect. 3.2.3.

3.2.2 Heated sensors

Measurements from two slower sensors, a heated Goodrich/Rosemount 102 sensor and a similar "Harco Model 100009-1 Deiced TAT" (HARCO) sensor, have also been evaluated, but only the latter is included here because they have similar response. The spectral variance for both these measurements has apparent rapid attenuation beginning at about 0.1 Hz, as shown in Fig. 6, and the response is attenuated seriously above about 1 Hz.

Attempts to use the same three-parameter representation of the transfer function relative to dynamic heating led to unsatisfactory fits, so a different approach is used here. Because the evaluation in Sect. 3.2.1 provides a good representation of the unheated Rosemount 102E4AL sensor, the measurements from that sensor, corrected as will be described in Appendix A, were used as the reference for the assumed-correct recovery temperature. Then the phase and amplitude ratio were found for the transfer function required to produce the heated-probe measurements from the unheated-probe measurements. This did not require any assumptions about equations or parameters determining the transfer function.

To characterize the response of the heated HARCO sensor, boundary-layer flight segments from the SOCRATES and CSET projects (referenced earlier in connection with the unheated probe) were compiled into one data set from the flight periods shown in Table 2. An unheated Rosemount 102E4AL sensor was also available, so corrected measurements from that sensor were used as the reference against which to determine the gain and phase of the transfer function.

The measured phase and amplitude ratio for this data set are shown in Fig. 7. The fit for the response function defined by (7) and (8) is shown as the blue line labeled "3-par" in that figure. The fitted values for $\{a, \tau_1, \tau_2\}$ were $\{0, 0.05, 1.12\}$, and to obtain this result the fit had to be constrained to keep a non-negative. A value of zero for the parameter a would indicate that no

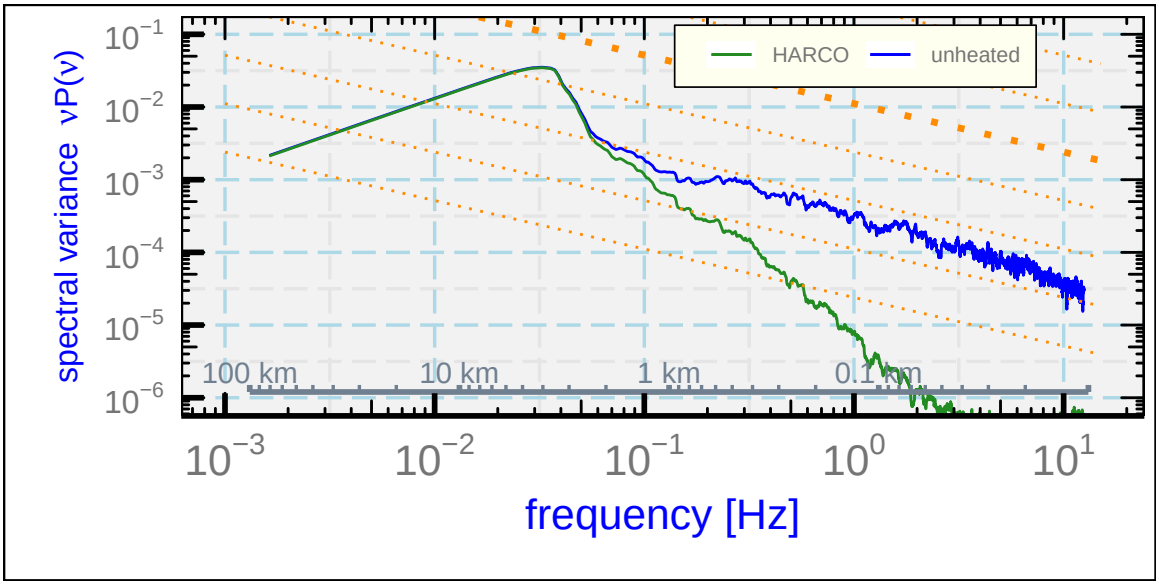

Figure 6: Spectral variance $P(v)$ weighted by frequency (v) for the recovery temperature measured by a heated HARCO and an unheated Rosemount sensor.

Project / Flight	start [UTC]	end [UTC]
CSET / 5	2015-07-14 17:52:00	18:02:00
CSET / 5	2015-07-14 19:45:30	19:55:30
CSET / 5	2015-07-14 20:37:17	20:47:17
SOCRATES / 15	2018-02-24 5:52:00	6:02:00
SOCRATES / 15	2018-02-24 6:05:00	6:15:00

Table 2: Flight segments used to determine the response characteristics of a heated HARCO sensor.

heat is transferred from the sensing wire to the air, but instead all is transferred to the support which has a relatively slow characteristic response.

The three-parameter fit is not consistent with the measurement errors even though it provides an approximate representation of the transfer function. The apparent reason is that there is conflict between the constraints imposed by the amplitude ratio and the phase, such that either could be represented reasonably but not both. The actual transfer function has some complex features, including frequencies where the phase shift reaches values below $-90°$ (not possible for a simple exponential time response) and values of the phase shift of about $-38°$ at 0.1 Hz where the amplitude ratio is still high (about 0.75). The amplitude decreases to e^{-1} at about 0.34 Hz, as would be the case for a first-order time constant of about 1.3 s, so this could be considered another measure of the response. However, that value does not extrapolate well to other frequencies and the phase shift at 0.34 Hz is approximately $-73°$, which would indicate that the measurement of a real contribution to sensible-heat flux at this frequency would be only about 10% of the correct value.

Because the three-parameter fit distorted the measured result, fits in the logarithm of the fre-

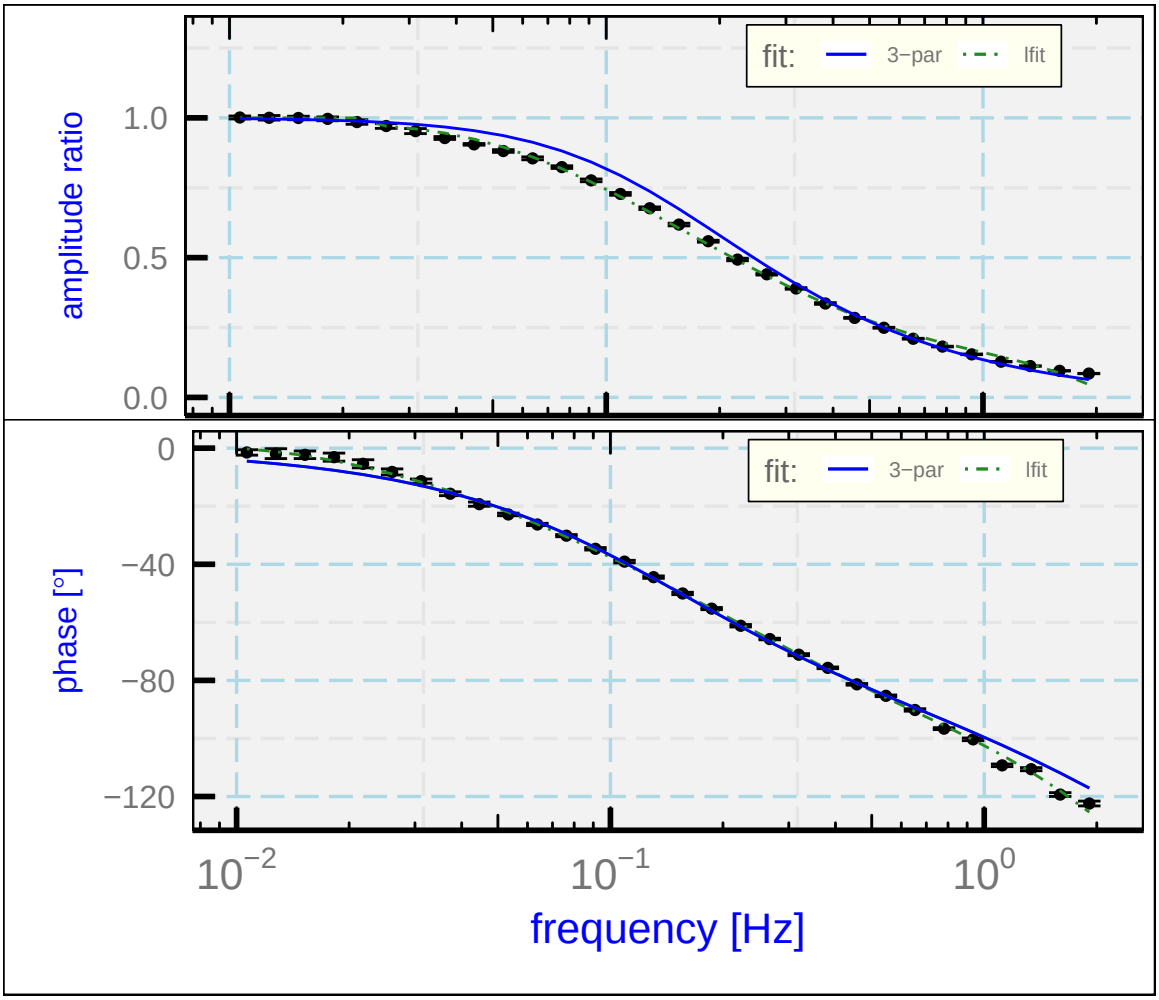

Figure 7: The gain (top) and phase (bottom) for the transfer function characterizing a heated HARCO temperature sensor. The measurements are indicated by error bars that show two-standard-deviation limits from the mean value). Two fits to the measurements, one based on the three-parameter representation ("3-par") and one on a polynomial fit ("lfit"), are described in the text.

quency were used to provide a better representation of the measurements, as shown by the dashed green lines labeled "lfit". Those fits are given by these equations and coefficients, with $x = \log_e(\nu/\nu_0)$ where ν is the frequency, $\omega = 2\pi\nu$ and $\nu_0 = 1\,\text{Hz}$:

$$\text{for } \nu > 0.024\,\text{Hz}, H(\omega) = (h_0 + h_1 x + h_2 x^3 + h_3 x^4 + h_4 x^5) e^{i\phi(\omega)} \tag{12}$$

$$\text{for } \nu \le 0.024\,\text{Hz}, \quad H(\omega) = 1$$

$$\phi(\omega) = p_0 + p_1 x + p_2 x^2 + p_3 \arctan(\nu/\nu_0)$$

The coefficients obtained by fitting to the observations are h_{0-4} ={0.161, −0.136, −0.0760, −0.0309, −0.00324} and p_{0-3} ={−155.2, −62.8, −6.35, 67.2}. This fit can be used to represent the transfer function better than the three-parameter fit (with negative-frequency values defined as the complex conjugate of the values at the corresponding positive frequency), although the fit needs to be modified above about 2 Hz because those values were not constrained by the measurements. A suggested modification is to duplicate the value at 2 Hz to higher frequencies; this appears to be adequate because there is so little variance measured by this sensor at these frequencies, but it is important to avoid possible zeroes that otherwise arise from extrapolation.

3.2.3 Expected dependence on flight conditions

Based on measurements in a wind tunnel, Stickney et al. [1994] indicated that the fast-response characteristic time τ_1 for the unheated Rosemount 102E4AL sensor varies approximately as $\log(Z^{-0.6})$ where $Z = M\rho_a/\rho_s$ with M the Mach number, ρ_a the air density and ρ_0 the air density under standard conditions. The mean value of Z for the flight segments used to find the best-fit parameters was $Z = 0.3$, so this suggests that the first characteristic time for that sensor is best represented by

$$\tau_1'(Z) = \tau_1 \left(\frac{0.3}{Z}\right)^{0.6} . \tag{13}$$

There is no similar evidence for τ_2, but it might be expected to have similar dependence because this is approximately the Reynolds number dependence and the Nusselt number characterizing ventilated heat transfer often is represented by a power-law relationship to the Reynolds number. If both heat transfer terms scale similarly, it might be expected that a will be unchanged.

For these reasons, the time parameters obtained in preceding sections have been adjusted to a reference value of $Z = 0.3$ in Table 3. For other conditions, it is suggested that the best estimate will be to multiply τ_1 and τ_2 by $(0.3/Z)^{0.6}$. (Having these parameters vary is in conflict with the "LTI" assumption leading to the transfer function, but these variations are minor over short times so incorporating this variation should produce reasonable results.)

sensor	a	τ_1 [s]	τ_2 [s]
unheated Rosemount 102E4ALon C-130	0.73	0.031	0.45
unheated Rosemount 102E4AL on GV	0.65	0.024	0.22
heated HARCO	0.0	0.058	1.29

Table 3: Parameters for the time response of available temperature sensors on the NSF/NCAR aircraft, adjusted to $Z = 0.3$. For other conditions, scale as represented for τ_1' in (13).

3.3 Response to a step change

The preceding subsection developed estimates of the sensor response with low uncertainty compared to previous estimates, so that will be the primary constraint on these parameters. It is nevertheless useful to check if other measurements that are sensitive to the time response are consistent with the characterization developed in the preceding subsections. Previous studies have mostly used sharp temperature changes in the atmosphere, for example from climbs through the inversion at the top of a boundary layer, to study the time response. A search of representative VOCALS climbs and descents through inversions capping the marine boundary layer found many with unusable structure but one near-ideal example, from VOCALS research flight 3, with a descent through the inversion at 8:13:50 UTC. Figure 8 shows the time history of the measured temperature for 8 s during this descent, which was at a rate of approximately 1000 ft/min (around 5 m/s). The temperature structure in this case was remarkably consistent with a near-constant temperature above the inversion and a near-adiabatic temperature structure below the inversion.

The suggested measurand history, if the discontinuity at the inversion is discrete, is that shown by the dashed black and dashed red lines.. The predicted time response from (4) for assumed time constants for the unheated Rosemount 102E4AL sensor adjusted for air density and flight speed is shown as the magenta line in Fig. 8. The predicted response is consistent with the observations and supports the approximate validity of the parameters determined from fits to the response to dynamic heating.

3.4 Application to a "speed run"

Another situation where a temperature lag can be observed is when the airspeed changes during level flight and causes a change in dynamic heating. An example is shown in Fig. 9, where the airspeed was increased steadily in level flight from near the lower limit of the flight envelope to near the upper limit and then was decreased back to the starting value. A plot of recovery temperature should also increase and decrease as the dynamic heating changes, but with a lag caused by the sensor response. This lag will produce hysteresis in the measured temperature during the speed run.

Figure **??**a shows this hysteresis, which appears as the difference between the segment with increasing speed and that with decreasing speed. A correction based on simply shifting the measurements in time works reasonably but doesn't take into account that the Mach number and hence the time parameters vary significantly during the speed run. A better test of the

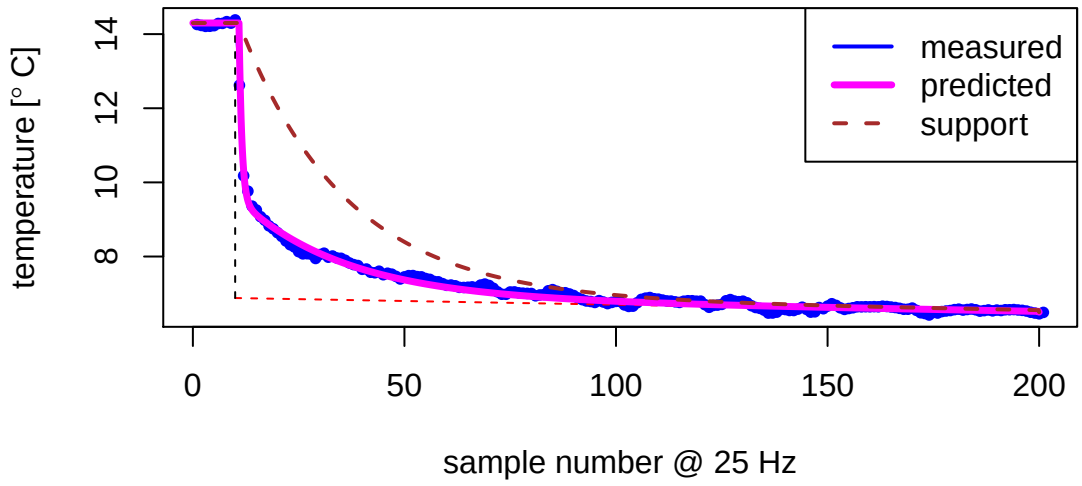

Figure 8: (blue dots): Temperature measured at 25 Hz during descent through an inversion capping the marine boundary layer, from VOCALS flight 3, starting at 8:13:50 UTC. The descent rate was approximately 5 m/s. The dashed red line shows a dry-adiabatic lapse rate in the marine boundary layer, and the dashed black line is a reference line indicating the location of the top of the boundary layer.The prediction using the parameters listed in the text is shown as the magenta line, mostly over the blue dots representing the measurements. The dashed brown line is the calculated temperature of the support that contacts the sensing wire.

time-response parameters is to apply the first correction scheme outlined in Appendix 2.2 to the measurements, with varying response parameters dependent on the Mach number. The specific correction equation used is (17). Figure 10b shows that the delay is mostly removed by this procedure. The residual standard deviation about the regression fit for recovery temperature as a function of $V^2/(2C_p)$ is reduced from 0.26°C before correction to 0.10°C after correction. The minimum standard deviation results from increasing the time constants an additional 10%, so measurements from this speed-run maneuver are consistent with the predicted time response as found in Sect. 3.2.2 to within about this uncertainty.

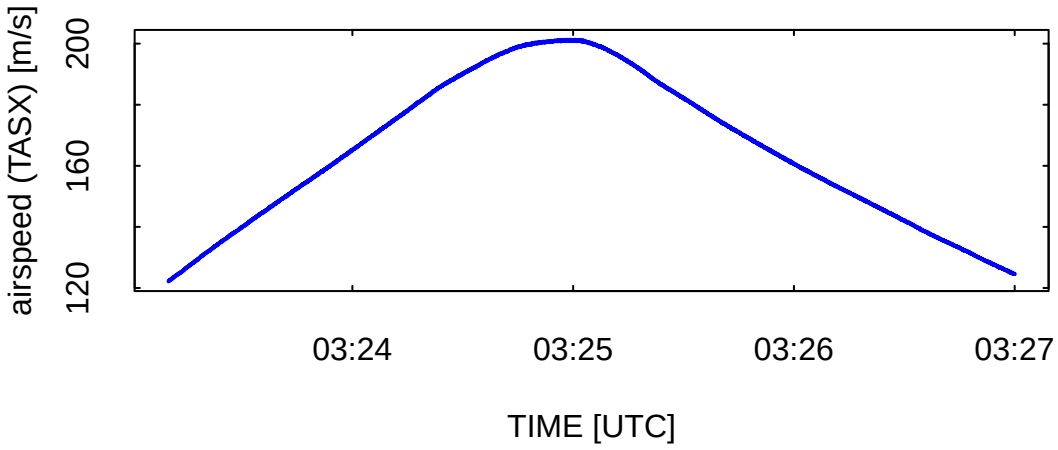

Figure 9: History of the airspeed during a "speed-run" maneuver where the airspeed varied during level flight over the available speed range of the aircraft.

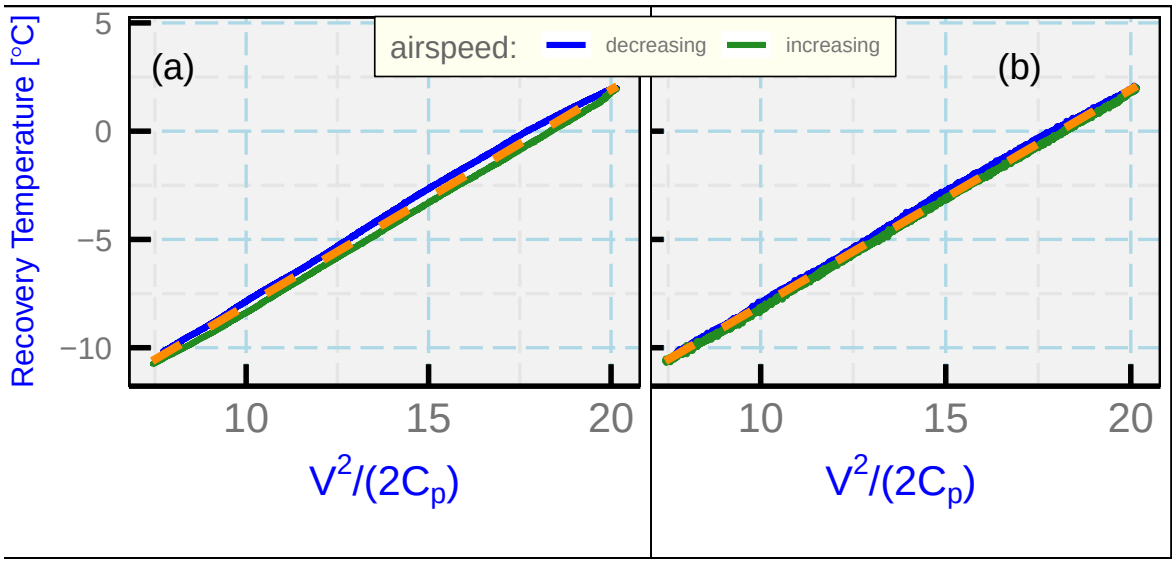

Figure 10: The recovery temperature as measured by a heated HARCO sensor during the speed-run maneuver shown in the previous figure (a) and the same measurement after correction (b). The abscissa is the dynamic-heating term without the recovery factor, where V is the airspeed and Cp is the specific heat at constant pressure. The measurements while the airspeed was increasing are shown by the green lines and those for decreasing airspeed by the blue lines. The dashed orange lines indicate the regression fits, with standard deviation about the fit of 0.26°C (uncorrected) and 0.10°C (after correction).

4 Uses of the Transfer Functions

The transfer functions determined in the preceding section have two potential uses: (i) to predict how airborne thermometers will respond; and (ii) to correct measurements to compensate for the time response of the sensors. The two papers that follow, Part 2 and Part 3, are examples of these two uses. In Part 2, the transfer functions are used to assess how sensors respond to dynamic heating and to develop appropriate correction schemes. Part 3 applies the transfer functions to improve measurements of the flux of sensible heat.

It is also possible to make corrections to the measurements for other purposes. Once the transfer functions are determined, the correction procedures use standard techniques, as discussed in Appendix A. These are suited to standard measurements made from most research aircraft and so can have general community utility.

5 Summary and Conclusions

Findings and conclusions of this investigation include these items:

1. The differential equations (3) and (4), with appropriate parameters, provide an analytical representation of the transfer function for the recovery temperature measured by an unheated Rosemount 102E4AL sensor. That transfer function was shown to be consistent with measurements of the phase and amplitude ratio of the response to dynamic-heating fluctuations. This is good evidence that the equations provide a good representation of the time response for that sensor. The predictions of the equations are less satisfactory when applied to a heated HARCO sensor or a heated Rosemount sensor, possibly indicating that the heat transfer is not represented adequately by those equations.

2. For the Rosemount 102E4AL sensor, the three parameters in those equations 9characterizing the two time constants and the fraction of heat transfer to the air vs. that to the structure supporting the sensing wire) can be determined with small uncertainty by fitting the transfer function to observations of dynamic heating. These parameters are thus constrained well and can be relied upon to make corrections to the measurements and otherwise to characterize the effects of time response of that sensor.

3. Some additional evidence supports the general magnitude of the parameters determined by reference to dynamic heating. The supplemental observations come from a sharp feature in the atmosphere and from the lag observed during flight while the airspeed varies at constant altitude.

4. Once the transfer function for the unheated Rosemount sensor has been determined, it can be used to estimate the true recovery temperature, and then transfer functions for other sensors can be determined by comparison to that estimate of the measurand to which they are responding. This approach has been used here for the slower heated sensors and should provide a means of correcting other sensors slower than the unheated sensor. Appendix A uses these results with standard methods to correct the measurements from airborne temperature sensors for their time response.

A Correcting the Temperature

The true recovery temperature T_r can be retrieved from the measured temperature T_m in two ways, either from the differential equations or by Fourier transformation. These methods are illustrated here.

The differential equations (3) and (4) provide a basis for correcting the measured temperature to account for the time response of the sensor. They should be applied to the recovery temperature $T_r(t)$, which is the measurand. The actual measurement is $T_m(t)$ and the temperature of the support is $T_s(t)$, so those equations, rearranged, are:

$$\frac{dT_s(t)}{dt} = \frac{T_r(t) - T_s(t)}{\tau_2} \tag{14}$$

$$T_r(t) = \frac{1}{a}\left\{\tau_1 \frac{dT_m(t)}{dt} + T_m(T) - (1-a)T_s(t)\right\} \tag{15}$$

There are two unknowns ($T_r(t)$, the actual recovery temperature, and $T_s(t)$). Those unknowns are specified by the two preceding equations because all other terms are known, including dT_m/dt which can be represented using the numerical derivative of the measurements $T_m(t)$. The second equation can be used to eliminate T_r from the first:

$$\frac{dT_s(t)}{dt} = \frac{\frac{1}{a}\left\{\tau_1 \frac{dT_m(t)}{dt} + T_m(T) - (1-a)T_s(t)\right\} - T_s(t)}{\tau_2} \tag{16}$$

From an initial value $T_s(0)$, assumed to be $T_m(0)$, this equation can be integrated to find the temperature of the support, $T_s(t)$. Once that is known, (15) specifies the estimate of the true recovery temperature $T_r(t)$ without further integration. The only choices needed are the numerical method used to find the derivative dT_m/dt (e.g., here centered fourth-order) and the integration method applied to (16), here fourth-order Runge-Kutta integration with Cash-Karp (Cash and Karp [1990]) adjustment of the step size. If a centered second-order finite-difference expression is used for $dT_m(t)/dt$ and an Euler integration is used to integrate (16), this correction can be shown to be equivalent to that developed by Inverarity [2000]; cf. his Eqn. (12).

An example of the corrected recovery temperature will be shown in the next subsection, where the two approaches to correction can be compared.

An alternate approach is to use Fourier transforms:

1. Calculate the Fourier transform of the measured time series: $\hat{T}_m(\omega) = \mathscr{F}\left(T_m(t)\right)$ where ω is the angular frequency and $\mathscr{F}$ denotes the Fourier transform.

2. Divide the result by the complex representation of the transfer function: $\hat{T}_r(\omega) = \hat{T}_m(\omega)/H(\omega)$.

3. Use the inverse Fourier transform to find a retrieved estimate of the true recovery temperature: $T_r(t) = \mathrm{Re}\left(\mathscr{F}^{-1}\left(\hat{T}_r(\omega)\right)\right)$ where Re denotes the real part of the complex result.

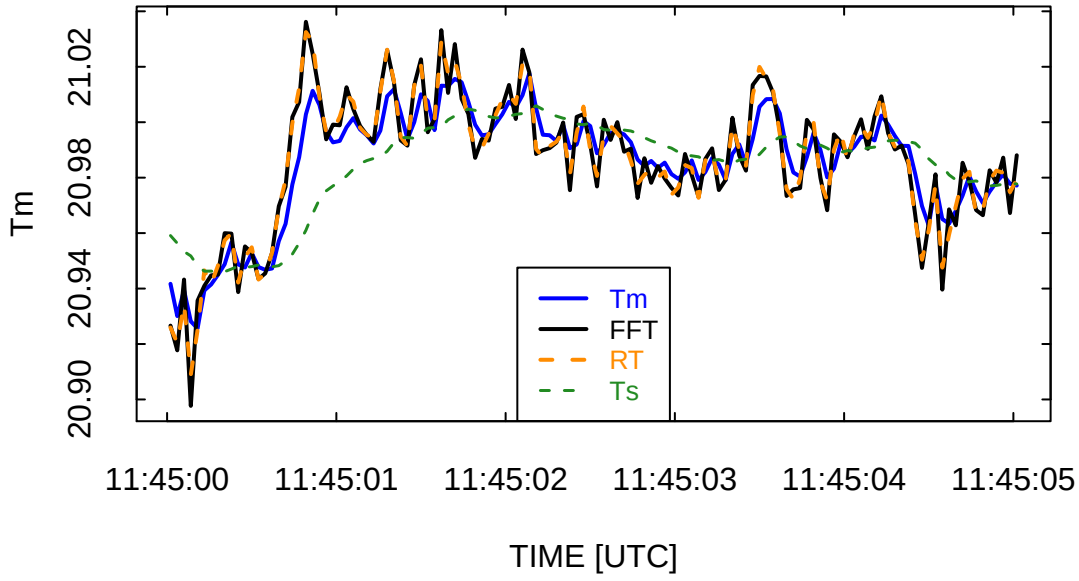

Figure 11: Example of the changes produced by the correction procedures. The original measurement of recovery temperature is Tm, produced by an unheated Rosemount sensor, and the revised values are RT (from integration) and FFT (from Fourier transforms). The dashed green line labeled "Ts" is the temperature of the support as calculated using (17). Measurements from VOCALS flight 3.

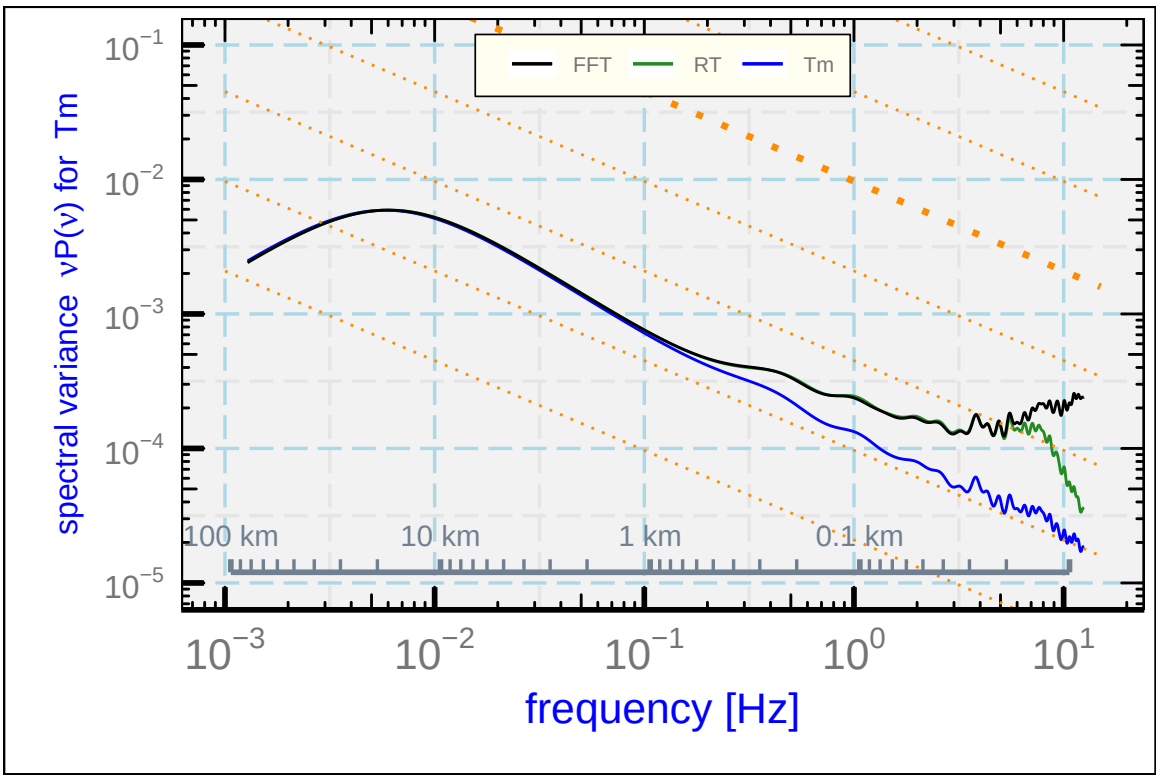

Figure 12: Variance spectra for the original measurement of recovery temperature (Tm) produced by an unheated Rosemount sensor and for the corrected values (RT and FFT) produced respectively by (16) and the Fourier-transform algorithm.

Sample results of these correction procedures are shown in Fig. 11. The agreement between the two correction methods is very good, and both show evidence of faster and higher-amplitude response to fluctuations. The resulting variance spectrum for the Fourier-transform method (Fig. 12) has high variance above about 5 Hz that is above the variance for the corrected variable obtained from (15). The increasing variance for the Fourier-transform method is is likely the fault of the measurement itself: The spectral variance for the original measurement (Tm) does not decrease at high frequency as expected from the transfer function, and the correction procedure amplifies this excess noise. The lower variance for the variable obtained from (15) at high frequency arises from the finite-difference representation of the term $dT_m(t)/dt$, which results in some smoothing.

Because the heated HARCO sensor is much slower than the unheated Rosemount 102E4AL sensor, the measurements from that slower sensor can't be corrected to the extent possible for the unheated sensor, but it is still useful to evaluate to what extent the measurements can be improved. The HARCO presents a special case because the best-fit value is $a = 0$ so (15) can't be used. However, in this case the differential equations can still be combined to give

$$T_r(t) = (\tau_1 + \tau_2)\frac{dT_m(t)}{dt} + T_m(t) + \tau_2\tau_1\frac{d^2T_m(t)}{dt^2} \tag{17}$$

a form that can be used directly without integration because finite-difference expressions can be used for the derivatives of the measured $T_m(t)$. The solution from (17) is very noisy if finite-difference estimates of the derivatives are used, so smoothing of the result was applied. Figure 13 shows the result (as "RTH") after a Butterworth low-pass filter with cutoff frequency of 2 Hz smoothed the corrected measurements. This filtering is reasonable because the variance spectrum for this sensor shows very little real signal at frequencies above 2 Hz. In comparison to the original measurement (labeled "Tm"), the response of the sensor is greatly improved by this correction procedure. It even provides a reasonable representation of the corrected unheated Rosemount measurement (labeled "RT") for the same period.

This is not as good a representation of the transfer function as is possible with the fitted representation shown in Fig. 7 and given by (12). That fit can be used with the Fourier-transform approach to correction. The result is shown in Fig. 13 as the black line labeled "FFT". This is also a significant improvement over the original and reproduces many of the features of the best measurement ("RT"). To obtain this result, it was necessary to attenuate frequencies above 1.8 Hz in the Fourier transform solution because there is a zero in the transfer function as represented by (12) that otherwise invalidates the inversion. This attenuation was accomplished by multiplying the transfer function by $e^{5\nu}$above 1.8 Hz. This arbitrarily chosen attenuation gave reasonable results, although it is likely that better choices could be made with further exploration. One more general measure of the improvement, beyond the anecdotal evidence in the preceding figures, is that either correction procedure reduced the standard deviation of the difference between the measured value (Tm) and the estimated best value (RT) from 0.06°C before correction to 0.03°C after correction.

The plot of variance spectra (Fig. 14) shows that the original spectrum (blue line labeled "Tm") is seriously attenuated at high frequencies relative to the reference measurement ("RT") and that both correction procedures restore significant parts of the missing spectral variance. Despite its inferior representation of the transfer function, it appears that application of 17 provides a

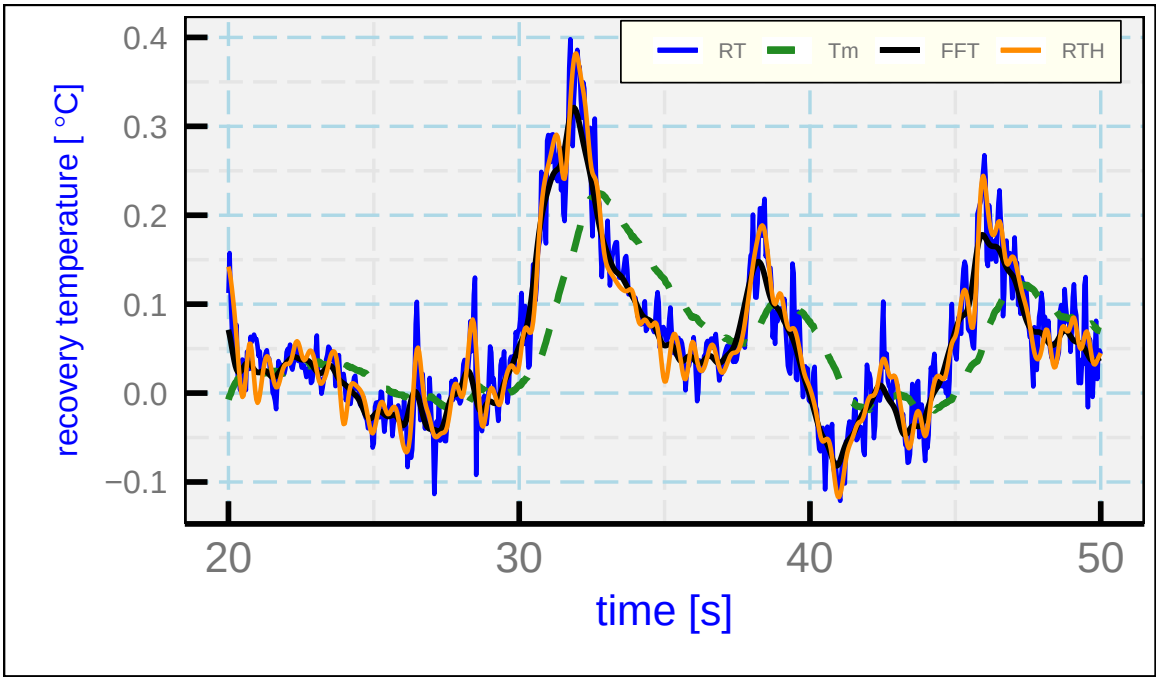

Figure 13: Corrected recovery temperature as measured by a heated HARCO sensor ("RTH" and "FFT"), the uncorrected measurement ("Tm"), and the best estimate of the true recovery temperature ("RT") based on an unheated Rosemount sensor after correction. The time is seconds after 2018-02-24 5:59:00 UTC, SOCRATES flight 15. "RTH" is based on the approximate formula (20), while "FFT" results from Fourier transformation after correction using the transfer function determined from (13). Mean values have been subtracted from all to facilitate comparisons.

better match to the reference measurements. It does not appear possible to restore the missing high-frequency fluctuations (above about 1 or 2 Hz) because the original measurement is so severely attenuated at these frequencies. This sensor and the similar heated Rosemount sensor are therefore unable to detect contributions to sensible-heat flux from this frequency range, even after corrections. It nevertheless appears useful to apply one of these correction approaches routinely to improve the quality of this measurement.

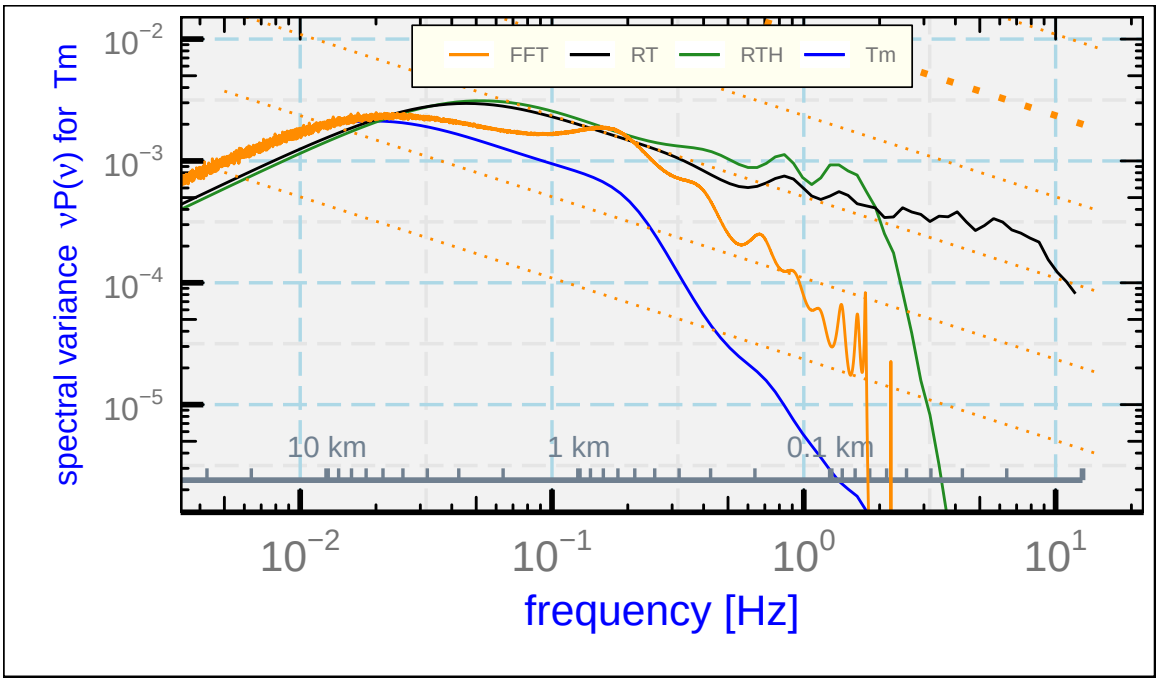

Figure 14: Variance spectra for some measurements of recovery temperature: "RT" (the best estimate resulting from correction of the measurements from the unheated Rosemount 102E4AL); "Tm" (the uncorrected measurement from the heated HARCO); "FFT" (the corrected HARCO measurement based on Fourier transforms); and "RTH" (the corrected HARCO measurement based on the correction formula (17)).

B Reproducibility

This document is constructed in ways that support duplication of the study. The code that generates the plots and implements the correction procedure is incorporated into the same file that generated this document via LaTeX, using principles and techniques described by Xie [2013] as implemented in the R package 'knitr' (Xie [2014]). The program, 'Paper1.Rnw', is archived on 'GitHub' in the directory at this URL. There is some supplemental material in that directory, including a workflow document for all the papers, the bibliography and some code segments saved in the "chunks" subdirectory, so the full directory should be downloaded in order to run the program. The calculations use the programming language R (R Core Team [2019]) and were run within RStudio (RStudio [2009]), so this is the most straightforward way to replicate the calculations and the generation of this document.

A package named Ranadu, containing auxillary functions, is used extensively in the R code. It is available on GitHub as https://github.com/WilliamCooper/Ranadu.git. The version used for calculations in this technical note is included in the 'zip' archive listed below.

The data files used are also preserved in the NCAR/EOL Data Archives and can be obtained via a request to `mailto:raf-dm@eol.ucar.edu` or via the "Data Access" links at this web site. The original files containing the data as produced by the NCAR Earth Observing Laboratory, Research Aviation Facility, were in netCDF format (cf. this URL), but in many cases data archives were reprocessed and the files may change after reprocessing so a separate archive is maintained for this document. The data files in this archive contain R data.frames and are preserved as binary-format 'Rdata' files via R 'save' commands. The code in the GitHub archive has appropriate 'load' commands to read these data files from a subdirectory named 'Data' (/Data or ~/Data or /home/Data) but this is not part of the GitHub repository because it is too large to be appropriate there. To reproduce this research, those data files have to be transferred separately from {??where??}

Extensive use has been made of attributes assigned to the data.frames and the variables in those data.frames. All the attributes from the original netCDF files have been transferred to the data.frames, so there is a record of how the original data were processed, for example with calibration coefficients and processing dependence for the variables. Key information like the processing date, the program version that produced the archive, and the selection of primary variables for various measurements thus is preserved.

(See the related list of project components on the next page that are preserved to enhance reproducibility.)

PROJECT:	SensibleHeatFlux
ARCHIVE PACKAGE:	SensibleHeatFluxPaper1.zip
CONTAINS:	attachment list below
PROGRAM:	Paper1.Rnw
ORIGINAL DATA:	UCAR/NCAR - Earth Observing Laboratory [2011], UCAR/NCAR - Earth Observing Laboratory [2017], ,UCAR/NCAR - Earth Observing Laboratory [2019]
SPECIAL DATA FILES:	SensibleHeatFluxTechNote.Rdata, SensibleHeatFluxTechNote2.Rdata
WORKFLOW DOCUMENT:	WorkflowSensibleHeatFlux.pdf
GIT:	https://github.com/WilliamCooper/SensibleHeatFlux.git

Attachments:
Paper1.Rnw
Paper1.pdf
WorkflowSensibleHeatFlux.pdf
WAC.bib
chunks/*
SessionInfo

References

Bruce Albrecht, Virendra Ghate, Johannes Mohrmann, Robert Wood, Paquita Zuidema, Christopher Bretherton, Christian Schwartz, Edwin Eloranta, Susanne Glienke, Shaunna Donaher, et al. Cloud system evolution in the trades (cset): Following the evolution of boundary layer cloud systems with the nsf–ncar gv. *Bulletin of the American Meteorological Society*, 100(1):93–121, 2019. (document), 3.1, 3.2.1

Jens Bange, Marco Esposito, Donald H. Lenschow, Philip R. A. Brown, Volker Dreiling, Andreas Giez, Larry Mahrt, Szymon P. Malinowski, Alfred R. Rodi, Raymond A. Shaw, Holger Siebert, Herman Smit, and Martin Zöger. *Measurement of Aircraft State and Thermodynamic and Dynamic Variables*, chapter 2, pages 7–75. John Wiley & Sons, Ltd, 2013. ISBN 9783527653218. doi: 10.1002/9783527653218.ch2. URL https://onlinelibrary.wiley.com/doi/abs/10.1002/9783527653218.ch2. 3

Jeff R Cash and Alan H Karp. A variable order runge-kutta method for initial value problems with rapidly varying right-hand sides. *ACM Transactions on Mathematical Software (TOMS)*, 16(3):201–222, 1990. A

W. A. Cooper, S. M. Spuler, M. Spowart, D. H. Lenschow, and R. B. Friesen. Calibrating airborne measurements of airspeed, pressure and temperature using a doppler laser air-motion sensor. *Atmospheric Measurement Techniques*, 7(9):3215–3231, 2014. doi: 10.5194/amt-7-3215-2014. URL http://www.atmos-meas-tech.net/7/3215/2014/. 3.1

W. A. Cooper, R. B. Friesen, M. Hayman, J. B. Jensen, D. H. Lenschow, P. A. Romashkin, A. J. Schanot, S. M. Spuler, J. L. Stith, and C. Wolff. Characterization of uncertainty in measurements of wind from the NSF/NCAR Gulfstream V research aircraft. NCAR technical note NCAR/TN-528+STR, Earth Observing Laboratory, NCAR, Boulder, CO, USA, jul 2016. URL http://n2t.net/ark:/85065/d7qr4zqr. 3.1

C. A. Friehe and D. Khelif. Fast-response aircraft temperature sensors. *J. Atmos. Ocean. Technol.*, 9(6):784–795, DEC 1992. ISSN 0739-0572. doi: 10.1175/1520-0426(1992)009<0784:FRATS>2.0.CO;2. 1, 2.1, 2.1, 3.1

G. W. Inverarity. Correcting airborne temperature data for lags introduced by instruments with two-time-constant responses. *Journal of Atmospheric and Oceanic Technology*, 17(2):176–184, 2000. doi: 10.1175/1520-0426(2000)017<0176:CATDFL>2.0.CO;2. URL https://doi.org/10.1175/1520-0426(2000)017<0176:CATDFL>2.0.CO;2. 2.1, A

R. Paul Lawson and Alfred R. Rodi. A new airborne thermometer for atmospheric and cloud physics research. part i: Design and preliminary flight tests. *Journal of Atmospheric and Oceanic Technology*, 9(5):556–574, 1992. doi: 10.1175/1520-0426(1992)009<0556:ANATFA>2.0.CO;2. URL https://doi.org/10.1175/1520-0426(1992)009<0556:ANATFA>2.0.CO;2. 1, 3.1

D. H. Lenschow. The measurement of air velocity and temperature using the NCAR Buffalo Aircraft Measuring System. Technical report, 1972. URL http://nldr.library.ucar.edu/repository/collections/TECH-NOTE-000-000-000-064. 2.1

John McCarthy. A method for correcting airborne temperature data for sensor response time. *Journal of Applied Meteorology*, 12(1):211–214, 1973. 2, 2.1, 2.1, 2.2

GM McFarquhar, R Wood, CS Bretherton, S Alexander, C Jakob, R Marchand, A Protat, P Quinn, ST Siems, and RA Weller. The southern ocean clouds, radiation, aerosol transport experimental study (socrates): An observational campaign for determining role of clouds, aerosols and radiation in climate system. In *AGU Fall Meeting Abstracts*, 2014. (document), 3.1, 3.2.1

National Research Council. *The Atmospheric Sciences: Entering the Twenty-First Century*. The National Academies Press, Washington, DC, 1998. ISBN 978-0-309-06415-6. doi: 10.17226/6021. URL https://www.nap.edu/catalog/6021/the-atmospheric-sciences-entering-the-twenty-first-century. 1

S Nicholls. Measurements of turbulence by an instrumented aircraft in a convective atmospheric boundary layer over the sea. *Quarterly Journal of the Royal Meteorological Society*, 104 (441):653–676, 1978. 2.2

G. A. Payne, C. A. Friehe, and D. K. Edwards. Time and frequency response of a resistance-wire aircraft atmospheric temperature sensor. *Journal of Atmospheric and Oceanic Technology*, 11(2):463–475, 1994. doi: 10.1175/1520-0426(1994)011<0463:TAFROA>2.0.CO;2. URL https://doi.org/10.1175/1520-0426(1994)011<0463:TAFROA>2.0.CO;2. 2, 2.1

David Pierce. *ncdf4: Interface to Unidata netCDF (Version 4 or Earlier) Format Data Files*, 2015. URL https://CRAN.R-project.org/package=ncdf4. R package version 1.15. (document)

R Core Team. *R: A language and environment for statistical computing*. R Foundation for Statistical Computing, Vienna, Austria, 2019. URL http://www.R-project.org. (document), 4, B

AR Rodi and PA Spyers-Duran. Analysis of time response of airborne temperature sensors. *Journal of Applied Meteorology*, 11(3):554–556, 1972. 2.1

RStudio. *RStudio: Integrated development environment for R (Version 0.98.879)*, 2009. URL http://www.rstudio.org. (document), B

T. M. Stickney, M. W. Shedlov, and D. I. Thompson. Goodrich total temperature sensors. Goodrich Technical Report 5755 Revision C, Rosemount Aerospace Inc., 1994. URL http://www.faam.ac.uk/index.php/component/docman/doc_download/47-rosemount-report-5755(lastaccess:8Aug2014). 3.2.3

Bruce Swihart and Jim Lindsey. *rmutil: Utilities for Nonlinear Regression and Repeated Measurements Models*, 2019. URL https://CRAN.R-project.org/package=rmutil. R package version 1.1.3. (document)

UCAR/NCAR - Earth Observing Laboratory. NCAR/NSF C-130 navigation, state parameter, and microphysics HRT (25 sps) data. version 1.0 [data set, VOCALS], 2011. URL https://doi.org/10.5065/d69k48jk,Accessed09Jan2020. (document), B

UCAR/NCAR - Earth Observing Laboratory. High rate (hrt - 25 sps) navigation, state parameter, and microphysics flight-level data. version 2.0. [data set, CSET], 2017. URL https://doi.org/10.5065/D63R0R3W,Accessed12Mar2020. B

UCAR/NCAR - Earth Observing Laboratory. High rate (HRT - 25 sps) navigation, state parameter, and microphysics flight-level data. version 0.1 [preliminary] [data set, WE-CAN], 2018. URL https://data.eol.ucar.edu/dataset/548.004.Accessed09Jan2020. (document)

UCAR/NCAR - Earth Observing Laboratory. High rate (HRT) navigation, state parameter, and microphysics flight level data. version 1.0 [data set, SOCRATES], 2019. URL https://doi.org/10.26023/K5VQ-K6KY-W610,Accessed09Jan2020. (document), B

H. Wickham. *ggplot2: elegant graphics for data analysis*. Springer New York, 2009. ISBN 978-0-387-98140-6. URL http://had.co.nz/ggplot2/book. (document)

R Wood, CR Mechoso, CS Bretherton, RA Weller, BJ Huebert, F Straneo, Bruce A Albrecht, H Coe, G Allen, G Vaughan, et al. The vamos ocean-cloud-atmosphere-land study regional experiment (vocals-rex): goals, platforms, and field operations. 2011. (document), 3.1, 3.2.1

Y. Xie. *Dynamic Documents with R and knitr*. Chapman and Hall/CRC, Boca Raton, Florida, 2013. URL http://yihui.name/knitr/. ISBN 978-1482203530. (document), B

Y. Xie. *knitr: A general-purpose package for dynamic report generation in R*, 2014. URL http://yihui.name/knitr/. R package version 1.6. (document), B